Instability and Treatments of the Coupled Discrete Element and Lattice Boltzmann Method by the Immersed Moving Boundary Scheme

Min Wang[1], Y.T. Feng[2], T.M. Qu[2], Tao Shi[3], T.T. Zhao[4]

1 T-3 Fluid Dynamics and Solid Mechanics Group, Theoretical Division, Los Alamos National Laboratory, Los Alamos, New Mexico 87545, USA

2 Zienkiewicz Centre for Computational Engineering, College of Engineering, Swansea University, Swansea, Wales SA1 8EP, UK

3 Key Laboratory of Distributed Energy Systems of Guangdong Province, Dongguan University of Technology, Dongguan 523808, China

4 Institute of applied mechanics and biomedical engineering, Taiyuan University of Technology, Taiyuan 030024, Shanxi, China

Abstract

The immersed moving boundary (IMB) scheme has been extensively used to couple the discrete element method (DEM) with the lattice Boltzmann method (LBM). In the literature, only the formulation of IMB for lattice nodal cells covered by a single solid particle was given. The treatment of situations where a nodal cell is covered by two or more solid particles is seldom discussed. It is found that some numerical instability can occur for such situations due to an inappropriate computation of the weighting function in the IMB formulation. This work presents an enhanced treatment that can resolve the issue and validates it using some benchmark tests. Furthermore, to avoid the extra costs associated with the treatment and simplify the complicated procedure introduced, a simplified IMB scheme is proposed. The accuracy of both enhanced and simplified IMB schemes are validated by test cases including single particle sedimentation, two-particle drafting-kissing-tumbling phenomenon and multiple-particle sedimentation. Then, the robustness of both schemes is examined and discussed using a specially designed flow past cylinders test. The simplified IMB scheme is proved to be robust and sufficiently accurate, and simpler and more effective than the enhanced scheme.

Keywords

Discrete Element Method; Lattice Boltzmann Method; Fluid-Particle Interaction; Immersed Moving Boundary; Multiphase Flow

List of symbols

f_i is the fluid density distribution function in the i^{th} direction;

x is the coordinate of the current lattice node;

$\mathbf{e}_i$ is the velocity vector in the i^{th} direction at the lattice node;

t is the current time;

C is the lattice speed;

h is the lattice spacing;

Δt is the time step for LBM;

Ω_i is a collision operator;

τ is the relaxation time;

$f_i^{eq}(x,t)$ is the equilibrium density distribution functions of fluid particles;

ω_i is the weighting factor in the i^{th} direction;

$\mathbf{u}$ is the physical fluid velocity;

ρ is the macroscopic fluid density;

ΔP is the fluid pressure;

ν is the fluid viscosity;

Ma is the Mach number;

$u_{\max}$ is the maximum magnitude of the velocity;

$\mathbf{u}_L$ is the fluid velocity in lattice system;

m is the mass of a solid particle;

I is the moment of inertia of a solid particle;

c is the damping coefficient;

$\mathbf{a}$ is the acceleration of a solid particle;

$\ddot{\theta}$ is the angular acceleration of a solid particle;

$\mathbf{F}_c$ is the contact force between two particles;

$\mathbf{T}_c$ is the torque caused by contact forces;

$\mathbf{F}_f$ is the hydrodynamic force applied to a solid particle;

$\mathbf{T}_f$ is the torque caused by hydrodynamic forces;

N_s is the sub-cycling number within a LBM time step;

Δt_{DEM} is the time step of DEM;

$\mathbf{F_i}$ is a body force term;

B_k is the weighting function of solid particle k;

ε_k is the ratio of the nodal cell area covered by the particle k to the total cell area;

ε_{total} is the summation of ε_k;

Ω_i^S is an additional collision term used for calculating hydrodynamic forces;

$\mathbf{U_s}$ is the velocity of a solid particle;

1 Introduction

The fluid-particle interaction is frequently encountered in various disciplines. Typical problems can be found in blood flow [1], piping erosion [2], fluidized bed [3], sand production [4] and many other particle-laden flow phenomena [5,6]. The computational fluid dynamics coupled with the discrete element method (CFD-DEM) has been widely employed to investigate such problems. From the viewpoint of the coupling process, CFD-DEM can be divided into two categories: the coarse-mesh technique [7,8] and the direct simulation [9,10]. In the former, a coarse fluid mesh in which each cell can accommodate about ten particles in the 2D case is adopted, but the hydrodynamic forces including drag, lift and pressure gradient forces acting on particles need to be calculated by semi-empirical equations. The latter direct numerical simulation approach, on the other hand, requires a very fine fluid mesh, whose size should be much smaller than the particles size, so that the hydrodynamic forces can be directly calculated by various immersed boundary methods. Obviously, the direct numerical simulation is of higher accuracy but more computationally expensive in general.

As an alternative to the conventional CFD, the lattice Boltzmann method (LBM) [11] based on the statistical mechanics has attracted considerable attention since 1990s due to its meso-scopic nature, easy to handle complex boundary conditions, and the explicit form of the time integration. Meanwhile, the collision process of fluid and solid particle nodes only occurs locally which makes LBM natural to be parallelized. Therefore, as a direct numerical simulation technique, the coupled discrete element and lattice Boltzmann method (DEM-LBM) becomes more and more popular for problems involving fluid-particle interactions [12-14].

Over the past three decades, several coupling schemes have been proposed to couple DEM and LBM. The modified half-way bounce-back method was the first attempt to simulate fluid-particle suspension in the frame of LBM in

1994 [15]. The hydrodynamic force was calculated by momentum exchange. This method was straightforward in modeling fluid-particle systems [2,16]. However, because of the step-wise boundary representation of solid particles, obvious oscillation of hydrodynamic forces computed by this method can be observed. To overcome the step-wise boundary profile, an interpolation-based approach [17,18,45] was developed, in which the solid boundary was represented by several boundary points. The density distribution functions of a boundary point before collision can be interpolated by its surrounding nodes and the density distribution functions after collision can be determined by momentum exchange. Finally, the density distribution functions of a fluid node can be interpolated from the solid boundary points and other surrounding fluid nodes. It is reported, however, that the no-slip boundary at the solid boundary is not always satisfied.

To solve this problem, the immersed boundary method (IBM) proposed in CFD by Peskin in 1977 [19] was introduced to LBM by Feng and Michaelides [20]. The basic idea of the IBM is to treat the particle boundary as a deformable body with high stiffness and represented by a set of discrete boundary nodes. The no-slip condition at the fluid-particle interface is satisfied by calculating the velocity of particle boundary points through interpolating fluid velocities on neighboring nodes. Then, momentum exchange and direct forcing-based IBM [21,22] were proposed. It is reported, however, that in this IBM-LBM the non-slip boundary condition is not fully enforced due to the explicit nature of forcing term formulation. Then, Wu and Shu [23] improved the IB-LBM using an implicit force density formulation where an unknown velocity correction is prescribed. This implicit scheme can enforce no-slip boundary at the fluid-solid interface but requires complex matrix inversion and a higher computational memory requirement. Recently, Dash et al. [24] proposed an implicit flexible forcing IBM by combining the implicit IB-LBM with a fixed multi-direct forcing IBM [25]. Instead of a fixed iteration number in the fixed multi-direct forcing IBM, a flexible sub-iteration for the velocity correction is terminated when the convergence limit is satisfied. However, oscillation of hydrodynamic forces can be found in this flexible implicit IBM, especially in flows with large Reynolds number [26].

To eliminate the obvious oscillation of hydrodynamic forces observed in the modified half-way bounce-back method, an immersed moving boundary (IMB) [27], also called the partially saturated method, was proposed. In this method, a weighting function associated with a nodal solid area was introduced to smoothly represent the boundary profile of a solid particle. In addition, to maintain the local collision characteristics, an additional collision term for nodes fully or partially covered by solid particles was introduced to the standard collision operator in LBM. Based on the momentum conservation, the hydrodynamic forces applied to the solid particle can be determined from the additional collision term. Because of its more accurate representation of the particle boundary, enhanced computational stability and reasonable efficiency, the IMB has been widely used in the coupled DEM-LBM technique where thousands of particles immersed in fluid can be modeled without difficulties [28].

The coupled DEM-LBM was first proposed by Cook et al. in 2000 [12,29]. In this seminal work, the IMB scheme was adopted to couple DEM and LBM, and particle suspension and erosion problems were simulated. Another classical work by Feng et. al. [30] developed an efficient DEM-LBM coupling framework where some key computational aspects, including the sub-cycling time integration, turbulent models and variable conversion between

the physical system and computational lattice system were provided and discussed in depth. Later, polygons or other general shaped solid particles were introduced into DEM-LBM [31, 32] in conjunction with IMB. Owen et al. [33] proposed a contact buffer to approximately consider the lubrication force between two particles so that the instability can be alleviated when two particles intersect at the same fluid nodal cell. Besides, different approximate methods, like cell decomposition and polygon approximation, were discussed for the calculation of a nodal solid area. Leonardi et al. [34] incorporated the non-Newtonian fluid model into the framework of DEM-LBM coupled by IMB. Later, the two-relaxation-time model was implemented into DEM-LBM and a modified weighting function for IMB was proposed to eliminate the relaxation time dependency of hydrodynamic forces [35]. In the same year, a searching algorithm for efficiently identifying boundary nodes was reported by Wang et al. [36], and the fast computation of a nodal solid area was proposed by Jones and Williams [37]. A more efficient searching algorithm and a Gaussian integration for calculating a nodal solid area were developed to improve the computing efficiency of DEM-LBM in our latest work [38,39]. Applications of this hybrid DEM-LBM-IMB technique can be found in hydraulic fracture [13,40], sand production [41,42], soil erosion [5], liquefaction [43] and immersed granular column collapse [44], to name a few.

Although a contact buffer was proposed in [33] to alleviate the instability issue when a nodal cell is covered by two or more particles, which is *termed the multiple-covered node* in what follows, it is insufficient to completely resolve the issue when particles move in relatively-large velocity in practical computation. This may result in the ratio of the total area of solid particles at *the multiple-covered node* to the nodal area exceeding 1.0. Consequently, a negative or extremely large weighting function can be encountered in the IMB and subsequently causes instability in LBM. To the best of the authors' knowledge, a detailed treatment of IMB in DEM-LBM for the situation where particles may overlap has not been reported. The current work aims at eliminating the instability issue of IMB encountered in multiple-covered nodes by introducing a special modification of the weighting function concerned. Then, to reduce the complexity and extra computing costs involved in the procedure, a simplified IMB scheme is proposed to model general fluid-particle systems. Only 2D cases are considered in the current work.

2 Coupled DEM and LBM

2.1 Lattice Boltzmann method

The lattice Boltzmann method is a modern numerical approach in computational fluid dynamics. In LBM the fluid domain is divided into regular lattices and the fluid phase is represented by a group of (imaginary) fluid particle packages resided at each lattice node (see Fig. 1). Each fluid particle package includes several fluid particles, such as the two-dimensional model with 9 fluid particles (so-called D2Q9). The fluid flow can be achieved through resolving the particle collision and streaming processes, and the lattice Boltzmann equation is used to solve the streaming and collision processes of fluid particles. Primary variables of LBM are the so-called fluid density distribution functions, which are portions of the fluid density, associated with the fluid particles. Both mass and momentum of fluid particles are characterized by the fluid density distribution functions. The detailed introduction of LBM can be referred to [11].

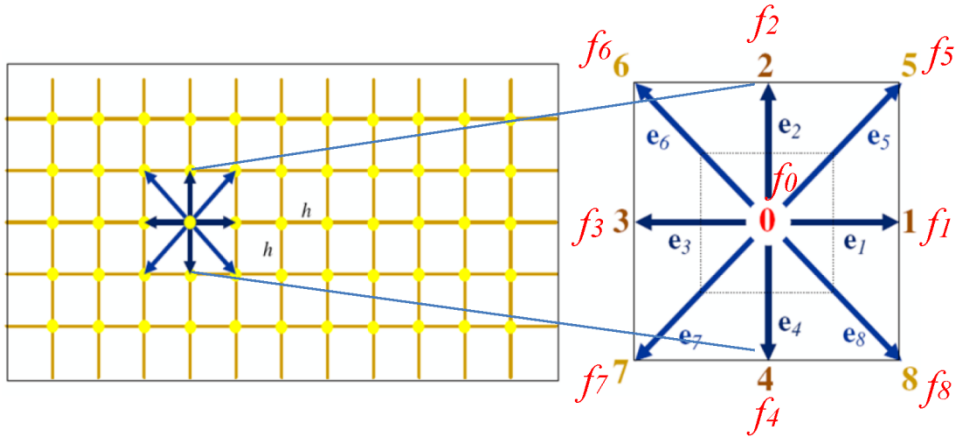

Fig. 1 Schematic of LBM with D2Q9 model

The lattice Boltzmann equation considering a body force is given by

$$f_i(x+\mathbf{e}_i\Delta t, t+\Delta t) - f_i(x,t) = \Omega_i + F_i\Delta t \tag{1}$$

where f_i is the fluid density distribution function in the i^{th} direction; x and $\mathbf{e}_i$ are the coordinates and velocity vectors at the current lattice node (see Fig. 1); t is the current time; F_i is body force term. The 9 velocity vectors ($\mathbf{e}_i, i = 0,8$) in the D2Q9 model are defined as

$$\mathbf{e}_0 = (0,0)$$

$$\mathbf{e}_i = C(\cos\frac{\pi(i-1)}{2}, \sin\frac{\pi(i-1)}{2}) \quad (i=1,...,4) \tag{2}$$

$$\mathbf{e}_i = \sqrt{2}C(\cos\frac{\pi(2i-9)}{4}, \sin\frac{\pi(2i-9)}{4}) \quad (i=5,...,8)$$

in which C is the lattice speed and is related to the lattice spacing, h, and the time step, Δt, by

$$C = h/\Delta t \tag{3}$$

Ω_i in Equation (1) is a collision operator. In the adopted Bhatnagar-Gross-Krook (BGK) [11] model, Ω_i is characterized by a relaxation time τ and the equilibrium density distribution functions $f_i^{eq}(x,t)$ of fluid particles at a certain velocity:

$$\Omega_i = -\frac{\Delta t}{\tau}\left[f_i(x,t) - f_i^{eq}(x,t)\right] \tag{4}$$

In this work, the D2Q9 model is adopted, and $f_i^{eq}(x,t)$ are defined as:

$$f_i^{eq} = \omega_i \rho(1 + \frac{3}{C^2}\mathbf{e_i}\cdot\mathbf{u} + \frac{9}{2C^4}(\mathbf{e_i}\cdot\mathbf{u})^2 - \frac{3}{2C^2}\mathbf{u}\cdot\mathbf{u}) \quad (i = 0,...,8) \tag{5}$$

where ω_i are the weighting factors:

$$\omega_0 = \frac{4}{9}, \quad \omega_{1,2,3,4} = \frac{1}{9}, \quad \omega_{5,6,7,8} = \frac{1}{36} \tag{6}$$

The corresponding fluid velocity $\mathbf{u}$ is

$$\rho\mathbf{u} = \sum_{i=1}^{8} f_i \mathbf{e_i} \tag{7}$$

where ρ is the macroscopic fluid density and given by

$$\rho = \sum_{i=0}^{8} f_i \tag{8}$$

The fluid pressure is given by

$$\Delta P = C_S^2 \Delta\rho \tag{9}$$

In the application of LBM, it is more convenient to choose τ and h as two independent parameters, then the time step, Δt, can be computed by

$$\Delta t = (\tau - \frac{1}{2})\frac{h^2}{3\nu} \tag{10}$$

where ν is the fluid viscosity.

It is obvious from Equation (10) that τ should be greater than 0.5, and Equation (9) indicates that the incompressibility of the fluid is not exactly enforced. The LBM can be viewed as a 'penalty-based' method that allows a limited degree of compressibility to occur where the 'speed of sound' in the fluid acts as a penalty value. The compressibility error is measured by the (numerical) Mach number (Ma)

$$Ma = \frac{u_{\max}}{C} \tag{11}$$

where $u_{\max}$ is the maximum magnitude of the velocity in the fluid domain.

In the practical simulation, a dimensionless lattice system is utilized to improve the computing efficiency. The conversion between physical quantities and those in the lattice system can be found in [30]. In the lattice system, the time step is equal to 1, and the fluid velocity $\mathbf{u}_L$ is scaled:

$$\mathbf{u}_L = \frac{\mathbf{u}}{C} \tag{12}$$

2.2 Sub-cycling coupling algorithm

In DEM the movement of each particle is updated by Newton's second law:

$$m\mathbf{a} + c\mathbf{v} = \mathbf{F}_c + \mathbf{F}_f + m\mathbf{g} \tag{13}$$

$$I\ddot{\boldsymbol{\theta}} = \mathbf{T}_c + \mathbf{T}_f \tag{14}$$

where m and I are respectively the mass and the moment of inertia of a solid particle, c is the damping coefficient, $\mathbf{a}$ and $\ddot{\boldsymbol{\theta}}$ are, respectively, the acceleration and angular acceleration of the particle; $\mathbf{F}_c$ and $\mathbf{T}_c$ are, respectively, the contact forces and corresponding torques; $\mathbf{F}_f$ and $\mathbf{T}_f$ are the hydrodynamic force and the corresponding torque. The lubrication force is not considered in this work.

The normal contact force is simulated by a linear spring model and the shearing force is calculated by the Coulomb friction model. Details of the contact model used in this work can be found in the work [30]. The time integration of DEM is achieved by the central difference method.

When coupling DEM with LBM, a sub-cycling time integration algorithm is employed. In general the time step of the DEM system is smaller than that of LBM. Therefore, in one LBM time step Δt, N_s sub-steps of DEM simulations will be performed:

$$N_s = \left\lceil \frac{\Delta t}{\Delta t_{DEM}} \right\rceil \tag{15}$$

where Δt_{DEM} is the time step of DEM, and $\lceil\ \rceil$ denotes an integer round-off operator.

2.3 Immersed moving boundary scheme

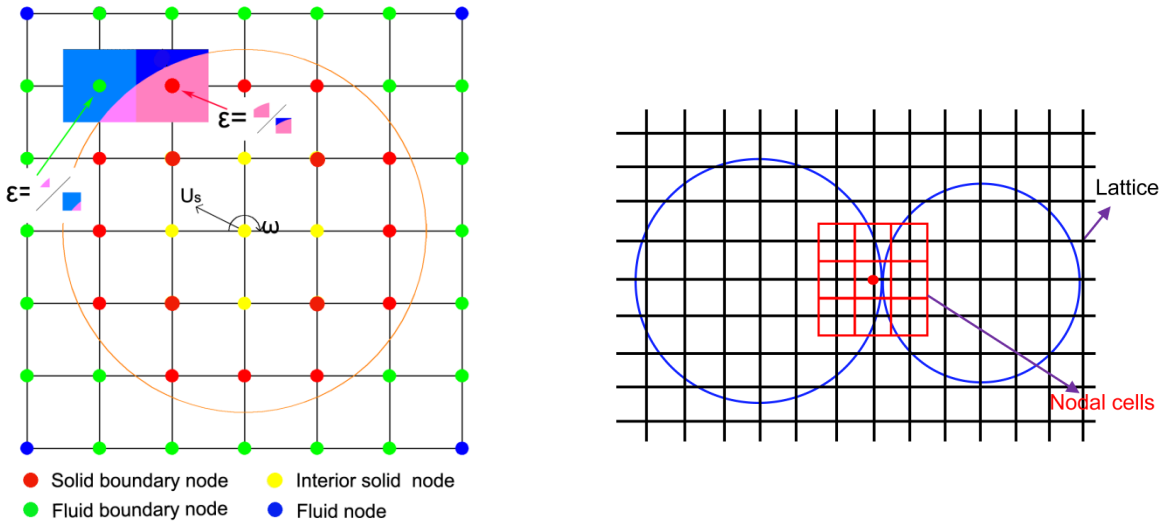

a. Simple case b. Complex case

Fig. 2 Diagram of IMB scheme

In the immersed moving boundary scheme [27], a solid particle is represented by the solid (lattice) nodes which are located within the particle. A solid node is called interior if its linked nodes are all solid nodes, while if a solid node has at least one linked fluid node, it is called a solid boundary node. A fluid node having at least one link to a solid node is defined as the fluid boundary node. Thus, there are four types of node in the IMB scheme: interior solid node, solid boundary node, fluid boundary node and normal fluid node, which are respectively marked in yellow, red, green and blue in an illustrative diagram of IMB in Fig. 2a. Each node is assigned a square cell of $h \times h$ (when using the lattice units, h = 1), called the *nodal cell*, and the node is located in the centre of the cell.

In order to retain the advantages of LBM, namely the locality of the collision operator and the simple linear streaming operator, an additional collision term, Ω_i^s, for the boundary nodes covered partially or fully by a solid particle is introduced to the standard collision operator of LBM. The modified collision operator [27] for resolving the fluid-solid interaction is given by

$$\Omega_i = -\frac{\Delta t}{\tau}(1-\sum_{k=1}^{n} B_k)[f_i(x,t) - f_i^{eq}(x,t)] + (1-\sum_{k=1}^{n} B_k)\Delta t \mathbf{F_i} + \sum_{k=1}^{n} B_k \Omega_i^S \tag{16}$$

where $\mathbf{F_i}$ is a body force term, B_k is the weighting function of solid particle k that depends on the local solid ratio ε_k which is defined as the ratio of the nodal cell area covered by the particle to the total cell area (see Fig. 2a); n is the number of particles covering the current nodal cell at x.

In some previous coupling schemes [2,15,16], the surface of a circular particle is represented by stepwise lattices, which is neither accurate nor smooth unless a sufficiently small lattice spacing is used. More seriously, when the particle is in motion, its boundary nodes will continually change, but in an 'on–off' fashion, which has serious implications in the computed interaction forces. It should be highlighted that compared to other coupling schemes mentioned in Introduction, the IMB scheme could smoothly represent the solid boundary during movement due to the incorporation of the weighting function B_k.

In the original IMB, the weighting function can be either in a linear form of the solid ratio

$$B_k = \varepsilon_k \tag{17}$$

or in a nonlinear form as

$$B_k = \frac{\varepsilon_k(\tau/\Delta t - 0.5)}{(1-\varepsilon_k) + (\tau/\Delta t - 0.5)} \tag{18}$$

When the lattice nodal cell is fully covered by fluid, $\varepsilon_k = 0$, the corresponding weighting function $B_k = 0$; When the nodal cell is fully occupied by a solid particle, $\varepsilon_k = 1$ and $B_k = 1$. This relation works only for the lattice node covered by a single solid particle. However, if a node is covered by multiple particles (see Fig. 2b), the weighting function should be different from Equation (18) and this complex situation was not mentioned in the literature [12,27,30,39]. Take the solid node marked by the red point in Fig. 2b for an example, the nodal cell marked by a red box is intersected by two particles. To satisfy the aforementioned relation between the solid ratio ε and the

weighting function B, the weighting function B_k of each solid particle intersecting with the lattice nodal cell should be defined as

$$B_k = \frac{\varepsilon_k(\tau/\Delta t - 0.5)}{(1-\varepsilon_{total}) + (\tau/\Delta t - 0.5)} \tag{19}$$

where

$$\varepsilon_{total} = \sum_{k=1}^{n} \varepsilon_k \tag{20}$$

Now when $\varepsilon_{total} = 0$, $\sum_{k=1}^{n} B_k = 0$; $\varepsilon_{total} = 1$, $\sum_{k=1}^{n} B_k = 1$.

Note that when the ratio of the total area of solid particles at the node to the nodal area ε_{total} exceeds 1, B_k should be defined as follows so that the summation of B_k will not exceed the limit 1.

$$B_k = \frac{\varepsilon_k}{\varepsilon_{total}} \tag{21}$$

The additional collision term is based on the bounce-back rule for the non-equilibrium part

$$\Omega_i^S = f_{-i}(x,t) - f_i(x,t) + f_i^{eq}(\rho, \mathbf{U_S}) - f_{-i}^{eq}(\rho, \mathbf{u}) \tag{22}$$

where $\mathbf{U_S}$ is equal to the velocity of the solid particle (see Fig. 2a) and $\mathbf{u}$ is the velocity of the fluid at the node. It should be highlighted that the selection of $\mathbf{U_S}$ is only valid for the node occupied by one solid particle. When multiple solid particles are present at this nodal cell, $\mathbf{U_S}$ should be the averaged velocity, defined as

$$\mathbf{U_S} = \frac{\sum_{k=1}^{n} \varepsilon_k \mathbf{U}_S^k}{\varepsilon_{total}} \tag{23}$$

The resultant hydrodynamic force and torque exerted on each solid particle can be calculated by

$$\mathbf{F}_f = Ch\Big[\ \sum_k (B_k \sum_i \Omega_i^s \mathbf{e}_i)\ \Big] \tag{24}$$

$$\mathbf{T}_f = Ch\Big\{\ \sum_k \big[(x - x_P) \times (B_k \sum_i \Omega_i^s \mathbf{e}_i)\big]\ \Big\} \tag{25}$$

Here the summation is over all nodes occupied by the solid particle under consideration.

The implementation of the above mentioned IMB scheme for nodes covered by multiple solid particles is not straightforward. The total number of solid particles presented in these nodal cells should be known before the relaxation of these nodes and the calculation of hydrodynamic forces applied to the corresponding solid particles. In addition to this added complexity, the computational CPU cost, which is one of the deficiencies of DEM-LBM, will further increase. From the latest report by Yang et al. [44] and our previous experience, when the size ratio of the (mean) particle diameter to the lattice spacing is greater than or equal to 20, numerical results are found insensitive

to the weighting function. To avoid the complicated treatment for special cases and expensive computational costs, we propose a simplified IMB as follows

$$\Omega_i = -\frac{\Delta t}{\tau}(1-B_k)[f_i(x,t)-f_i^{eq}(x,t)]+(1-B_k)\Delta t\mathbf{F_i}+B_k\Omega_i^S \tag{26}$$

In this simplification, the summation $\sum_{k=1}^{n} B_k$ of the weighting functions in Equation (16) is replaced by B_k. In the actual implementation, the relaxation of both fluid and solid boundary nodes is performed under the loop of solid particles. B_k is taken to be the weighting function of an arbitrary solid particle that is intersecting with the nodal cell, for instance, the particle with the greatest ID. The hydrodynamic force and corresponding torque applied to the solid particle can be computed by Equations (24) and (25). However, to comply with the principle of momentum conservation, the weighting function used here should be Equation (18) rather than (19) and (21). Now there are three different IMB schemes which are compared in Table 1. Their performance in terms of accuracy and computational cost will be examined in the next section.

Table 1 Comparison of different IMB schemes

	Collision operator	**Weighting function**	**Solid velocity**
Original IMB	Equation (16)	Equation (17) for linear Equation (18) for nonlinear	-
Enhanced IMB	Equation (16)	Equation (17) for linear Equations (19-21) for nonlinear	Equation (23)
Simplified IMB	Equation (26)	Equation (17) for linear Equation (18) for nonlinear	-

3 Numerical examples and validations

In this section, a series of numerical tests with increasing complexity are carried out to validate and compare the three different forms of the weighting function. First, the extensively-investigated single particle sedimentation is modelled using both linear and nonlinear weighting functions. Then, two-particle drafting-kissing-tumbling (DKT) phenomenon is performed to further validate the accuracy of the weighting functions for the enhanced and simplified IMB. Next, a multiple-particle sedimentation case is used to check the applicability and accuracy of the enhanced and simplified IMB. Finally, a special flow past cylinders case, where two moving particles behind a stationary cylinder may have a large overlap, is further carried out to demonstrate the robustness of the proposed schemes.

3.1 Single particle sedimentation

This benchmark is the most commonly used to validate the accuracy of IMB in DEM-LBM simulations. A stationary solid particle with diameter 0.25 cm is located at the position (1 cm, 4 cm) in a tube 2 cm width and 6 cm

height at the beginning of simulation. The densities of the solid particle and the fluid are respectively 1.25 g/cm^3 and 1.0 g/cm^3. The kinematic velocity of the fluid is 10^{-5} m^2/s. In the simulation, the relaxation time 0.65 is selected and the lattice spacing (h) is 0.01 cm so that the ratio (25) of the particle diameter to the lattice spacing is greater than 20 which is the minimum value for an accurate simulation in DEM-LBM. The time step for LBM and DEM has the same value 10^{-5} s. Due to the gravity force, the particle will move downward. Because the simplified IMB and enhanced IMB are the same for simulating a single particle, only the linear and nonlinear weighting functions proposed in [27] are, respectively, employed and compared with the result obtained by the direct numerical simulation of CFD [45].

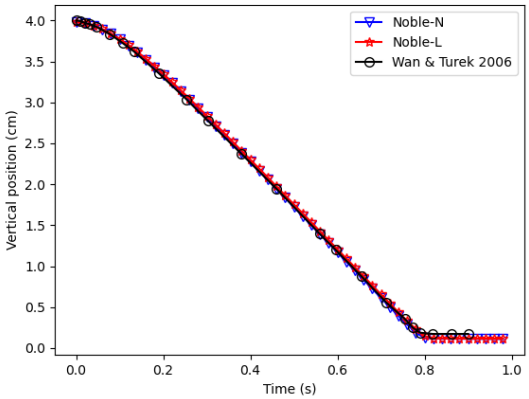

a. Variation of particle vertical position

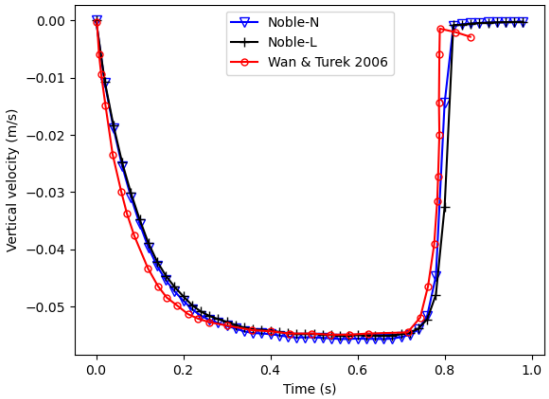

b. Variation of particle vertical velocity

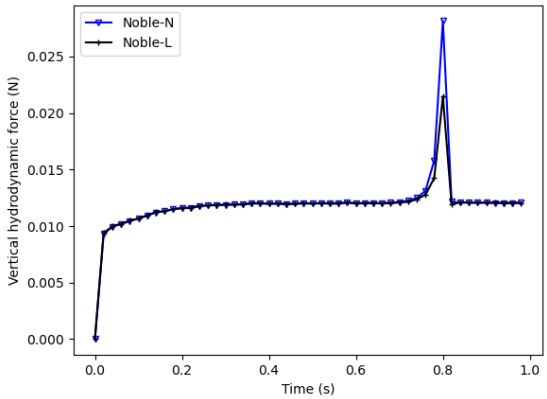

c. Comparison of variation of hydrodynamic forces

Fig. 3 Comparison of particle position, velocity and hydrodynamic forces simulated by linear and nonlinear weighting functions

Figures 3a and 3b compare the variation of both vertical position and velocity of the solid particle over time, respectively. It is found that the motion of the particle obtained by both linear and nonlinear weighting functions is

the same and matches the CDF simulation [45] in Figure 3a. A slight difference between the velocity of the CFD and IMB simulations can be observed. Because the hydrodynamic force in the CFD simulation is not available, only the hydrodynamic forces obtained by both linear and nonlinear weighting function are compared in Figure 3c. They are almost the same except after the particle collides with the bottom boundary. From this benchmark, there seems no obvious difference between the linear and nonlinear weighting functions in the IMB scheme.

3.2 Two-particle DKT simulation

To check the accuracy of the simplified IMB and further compare the accuracy of the linear and nonlinear weighting functions in the enhanced IMB, the well-known DKT phenomenon is selected as the second benchmark test. A rectangular box of size 2 cm by 8 cm is filled with water. The fluid density and kinematic viscosity are 1.0 g/cm^3 and 10^{-6} m^2/s respectively. Initially, two particles with the same diameter (0.2 cm) and density (1.01 g/cm^3) are placed, respectively, at positions (1.0 cm, 7.2 cm) and (1.0 cm, 6.8 cm). The relaxation time and lattice spacing (h) are selected as 0.65 and 0.01 cm. The time step of LBM is 5×10^{-4} s and the sub-cycling number (N_s) of DEM within one LBM time step is 47. Lattices around particles are shown in Figure 4. To simulate the lubrication force, a contact buffer ($0.3h$) is adopted in our code and the contact stiffness between solid particles is 10^7 N/m. These two particles will fall under gravity force. Then, a well-known drafting-kissing-tumbling phenomenon should be observed, but only in the simulation using the nonlinear weighting function.

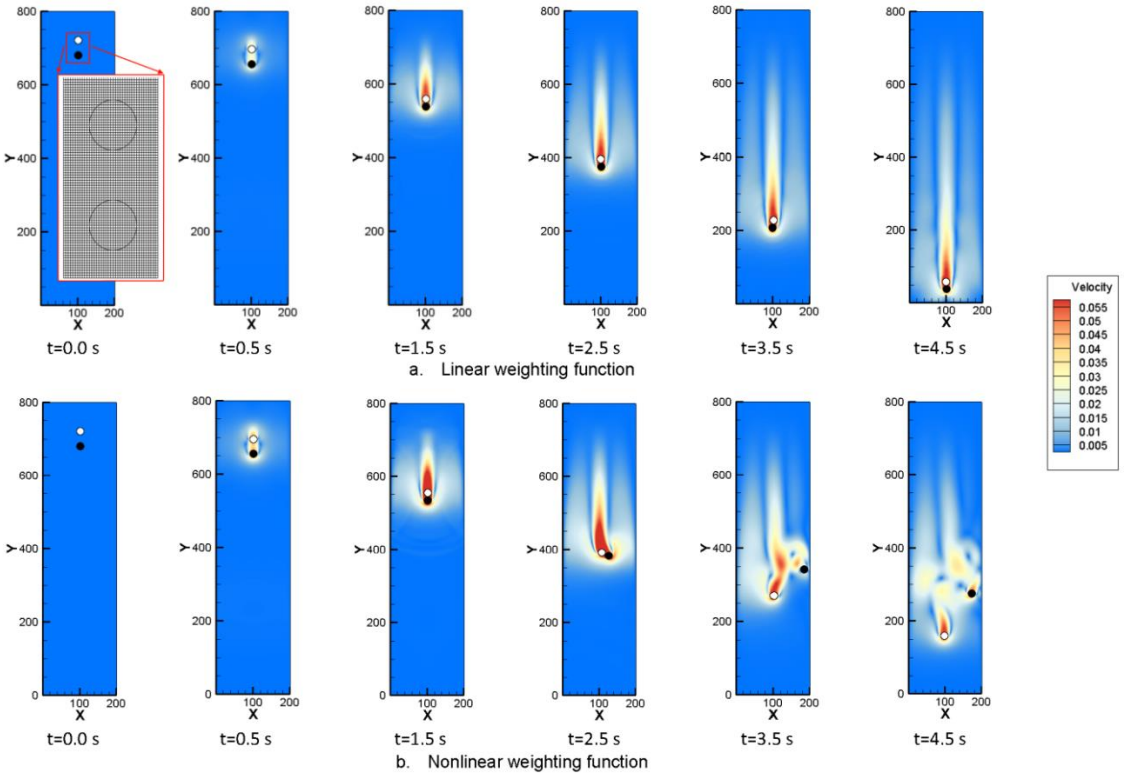

Fig. 4 Comparison of fluid velocities and particle positions at different time instants for linear (a) and nonlinear (b) weighting functions

Figure 4 shows the instantaneous particle positions and the velocity contours of the fluid flow at different time instants. In the legend, the magnitude of the fluid velocity in the lattice system is given, because the maximum fluid velocity in the lattice system is the Mach number which measures fluid compressibility. As the Mach number is smaller than 0.1, the simulation can be regarded as reliable. It is found that the linear weighting function cannot recover the DKT process, though it works well for the single particle case. In contrast, the enhanced IMB with nonlinear weight function and our simplified IMB succeed in simulating the intended phenomenon. Figure 5 depicts the vertical and horizontal variations of the particle positions and compares them with some existing results obtained by different IBM simulations [20,21]. It can be seen that almost no difference in the particle position is observed between the enhanced IMB with the nonlinear weight function and the simplified IMB, and both are similar to the result of [21]. Then, the high-order results, velocity and hydrodynamic forces, of the two particles obtained by different IMB schemes are compared in Figures 6 and 7. A slight difference in the vertical velocity and the hydrodynamic force can be seen, but an obvious difference in the horizontal hydrodynamic forces can be observed when the top particle approaches the other one.

It should be highlighted that in the current DEM-LBM development most researchers only use the single particle sedimentation as the quantitative benchmark, and this DKT case proves that the single particle sedimentation may be insufficient to validate different IMB schemes. In addition, comparison of hydrodynamic forces obtained from different coupling schemes may tell more story than the commonly used position and velocity. However, hydrodynamic forces were seldom given in the literature. Our recent work [26] reported that some IBM schemes are capable of obtaining smooth profiles of particle position and velocity but unexpected oscillation of computed hydrodynamic forces can be found.

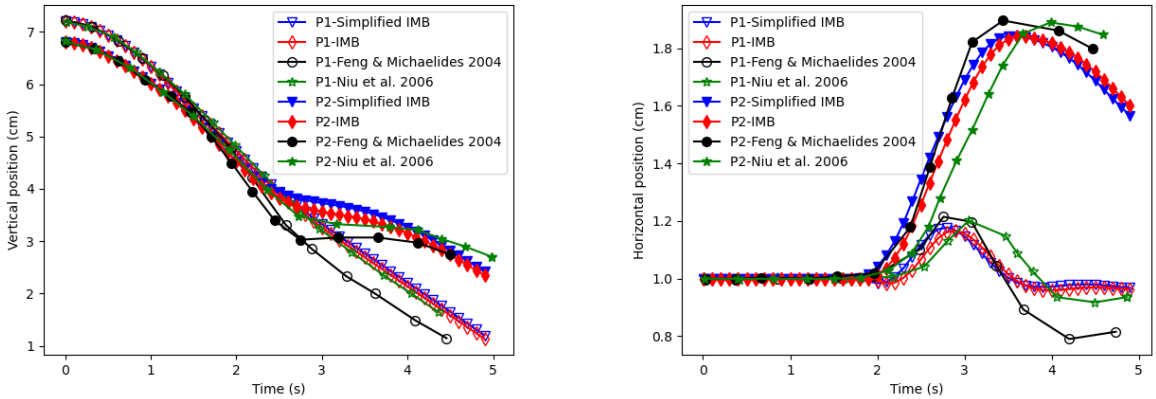

a. vertical position

b. horizontal position

Fig. 5 Variation of particle positions in DKT (P1 - top particle; P2 – bottom particle)

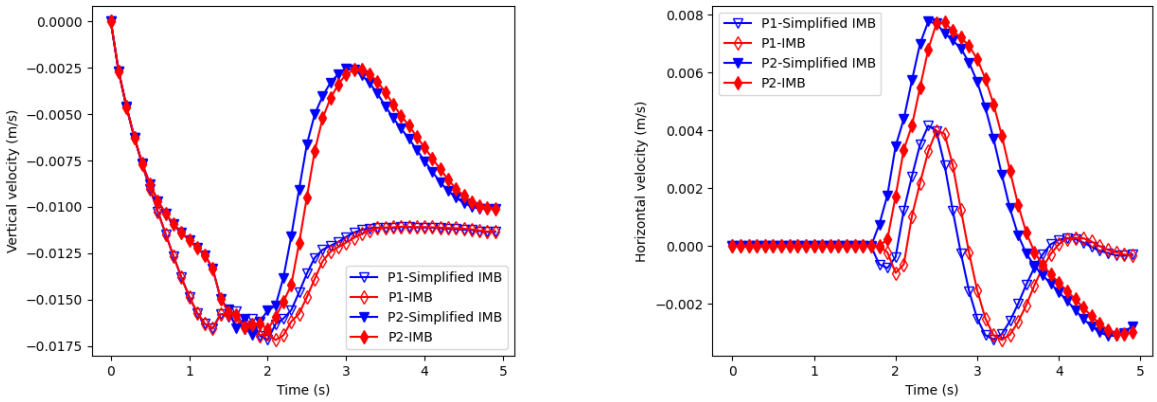

a. Variation of vertical velocity

b. Variation of horizontal velocity

Fig. 6 Variation of particle velocities in DKT

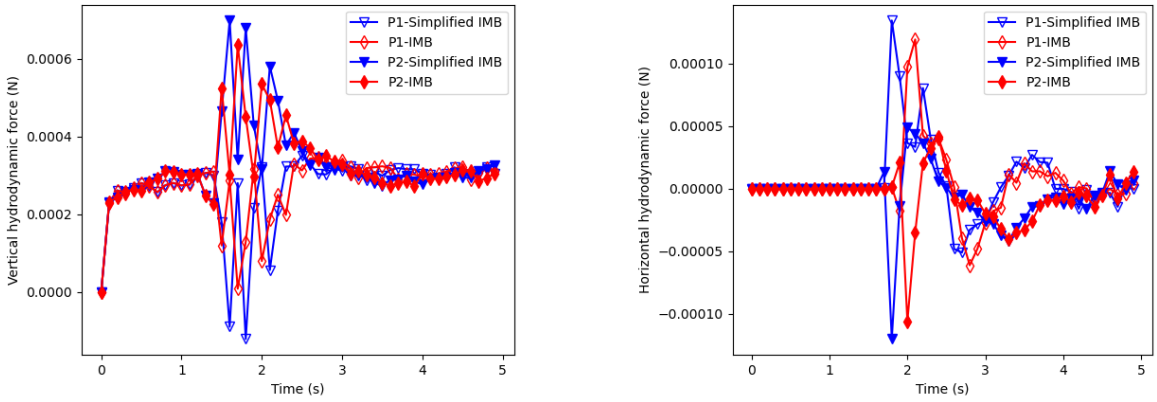

a. Variation of vertical hydrodynamic forces

b. Variation of horizontal hydrodynamic forces

Fig. 7 Variation of hydrodynamic forces applied to particles in DKT

3.3 Multiple-particle sedimentation

To further examine the applicability of the enhanced and simplified IMB schemes for problems with potential multiple-covered nodes, the multiple-particle sedimentation of particles with two different sizes are carried out, in which the particles can be in contact with each other. The diameters of white and black particles are respectively 0.2 cm and 0.3 cm, and their contact stiffness and density are respectively 10^7 N/m and 3.0 g/cm^3. The fluid density and kinematic viscosity are respectively 1.0 g/cm^3 and 10^{-5} m^2/s. The relaxation time and lattice spacing are selected as 0.501 and 0.01 cm, respectively. The time step for LBM and DEM has the same value 3.33×10^{-7} s. The no-slip boundary is applied to the four boundaries. At the beginning all the particles are stationary and they start to fall under gravity.

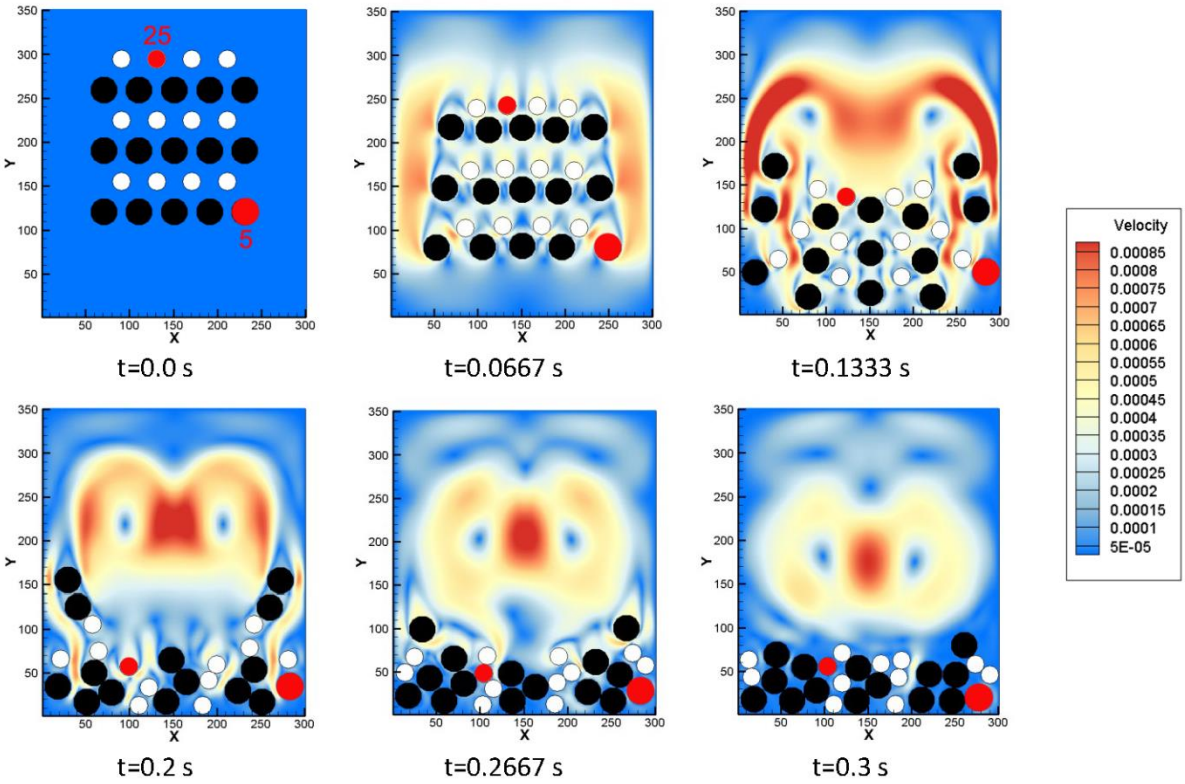

Fig. 8 Contour of fluid velocity and position of particles of multiple-particle sedimentation at different time instants

361
362

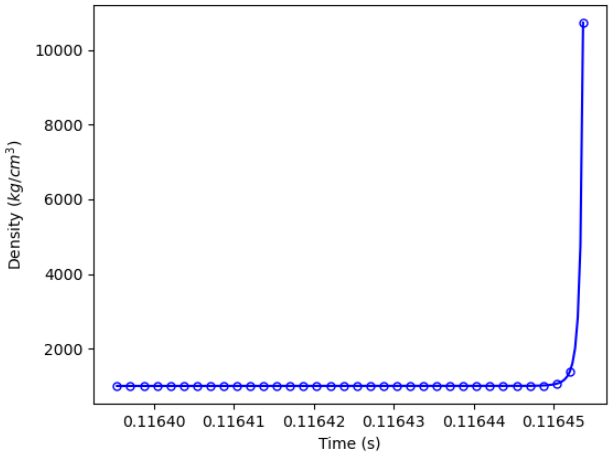

Fig. 9 Abnormal variation of fluid density at node (217,30) over time

363

364

Figure 8 shows the snapshots of the velocity contour of the fluid and the distribution of the solid particles at different time instants. Again, the magnitude of fluid velocity in the lattice system is given here and in the other examples below. During the sedimentation process, many particles collide with others, and the multiple-covered grid nodes are encountered. Figure 9 shows the abnormal variation of fluid density at node (217, 30) before the simulation using the original IMB crashes. With the enhanced IMB, the instability of original IMB can be resolved. Detailed discussion on instability of the original IMB scheme will be given in the next section. Both the enhanced and simplified IMB can successfully simulate this problem.

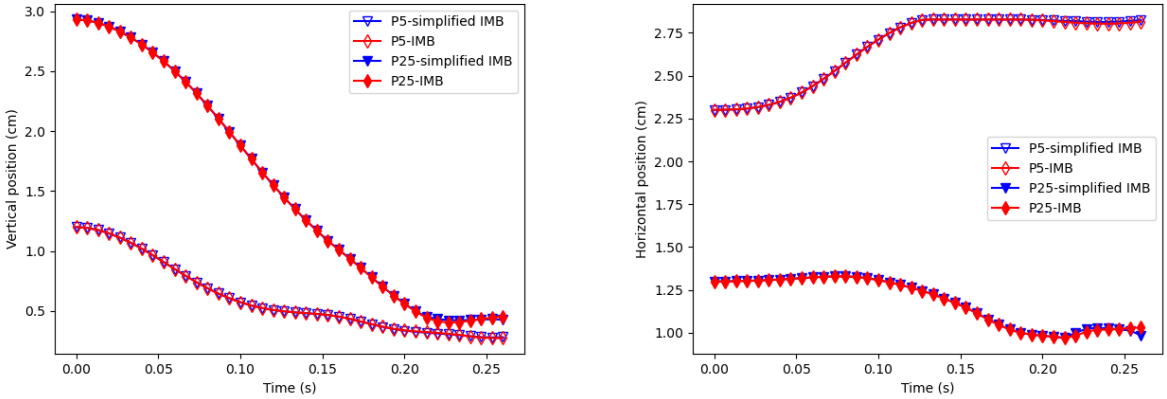

a. Vertical position of particles

b. Horizontal position of particles

Fig. 10 Comparison of particle positions over time

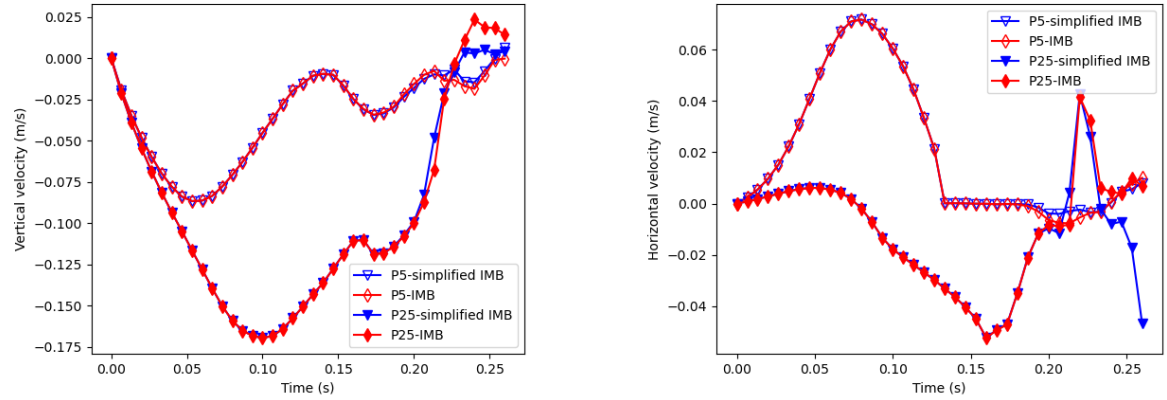

a. Variation of vertical velocity of particles

b. Variation of horizontal velocity of particles

Fig. 11 Comparison of particle velocities over time

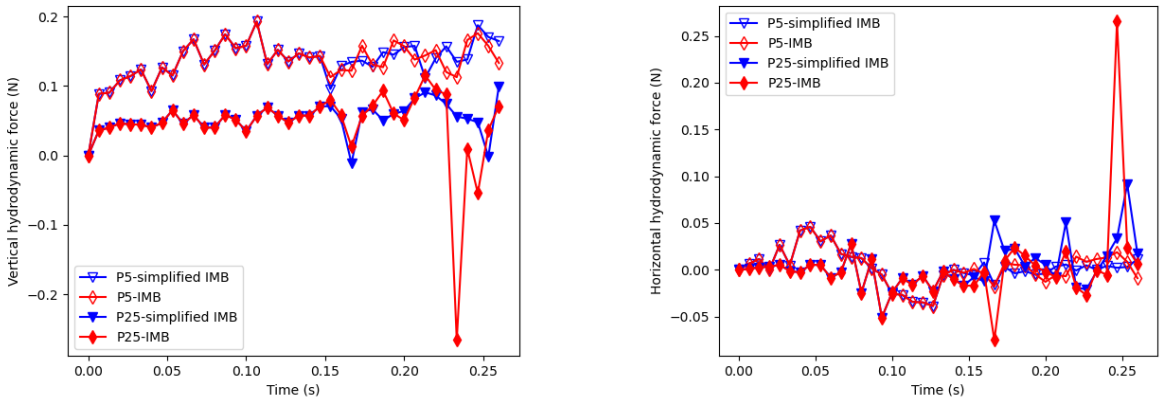

a. Comparison of vertical hydrodynamic forces b. Comparison of horizontal hydrodynamic forces

Fig. 12 Comparison of hydrodynamic forces applied to solid particles

To quantitatively compare the two schemes, the time histories of positions, velocities and hydrodynamic forces of two randomly selected particles in red (5^{th} and 25^{th}) are given in Figures 10 to 12. Similar to the finding in the DKT simulation, the position profiles of the two particles are almost the same. Differences between their velocities and hydrodynamic forces can be observed when particles are in contact with others. This example further indicates that the velocity and, especially, hydrodynamic force should be examined as quantitative validations. Overall, the simplified and enhanced IMB schemes are in good agreement for this test case.

3.4 Special flow past cylinders

This test case is a specially designed flow past cylinders problem consisting of three white particles representing three fixed cylinders, and two black particles departing from each other first and then moving vertically towards each other with the same fixed speed (0.0003 cm/s). A pressure gradient between the left inlet and the right outlet is achieved by specifying two different densities at the inlet and outlet ($\rho_{in} = 1000.1 kg/m^3$ and $\rho_{out} = 1000 kg/m^3$). The diameter of all particles is 20 cm, and their contact stiffness and density are 10^6 N/m and 3.0 g/cm^3. The fluid density and kinematic viscosity are 1.0 g/cm^3 and 10^{-5} m^2/s. The time step for LBM and DEM has the same value 0.03 s. The relaxation time and lattice spacing are selected as 0.6 and 1 cm, respectively. This test is designed to examine the stability issue of the enhanced IMB and the robustness of the simplified IMB.

In the first stage (t <= 3333s), the two black particles depart from each other until they are in (slight) overlap with a white cylinder. In a later stage, the two back particles will move toward each other until they are fully overlapped. Thus some multiple-covered nodes are expected to be encountered.

Figure 13 shows the velocity contour of the fluid flow at different time instants obtained by the simplified IMB. Smooth and stable fluid flow patterns are observed here.

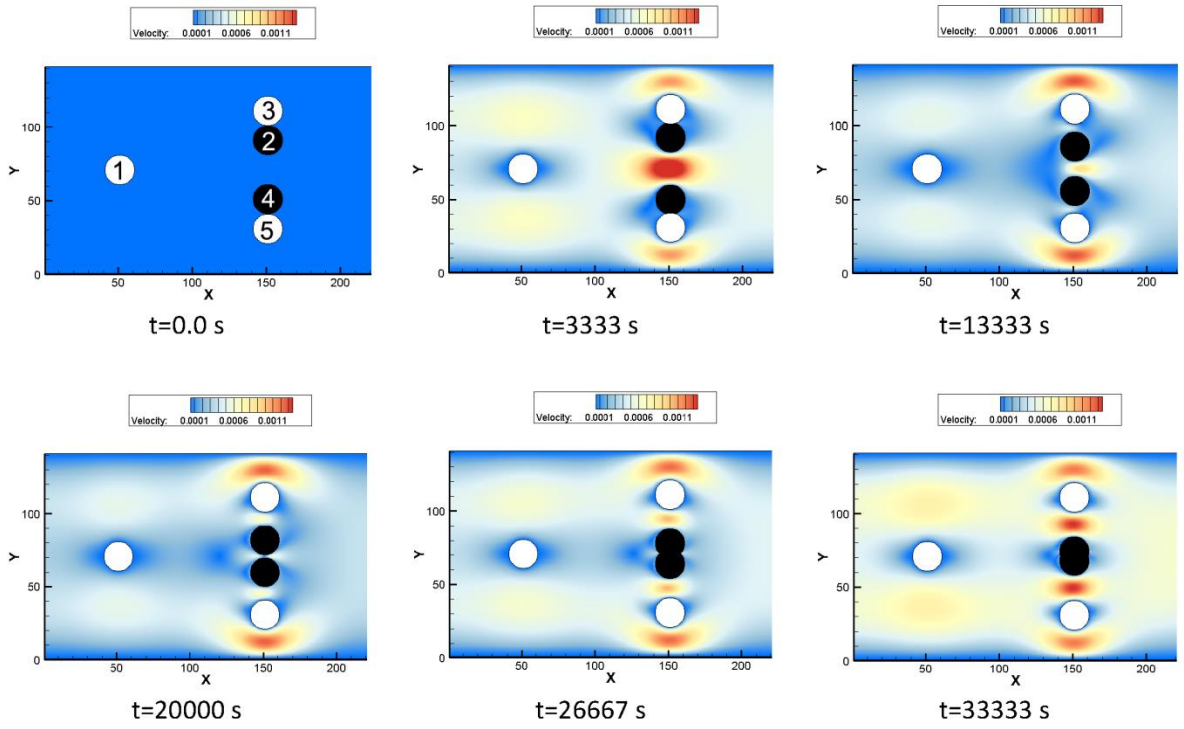

Fig. 13 Contour of fluid velocity at different time instants

397
398
399

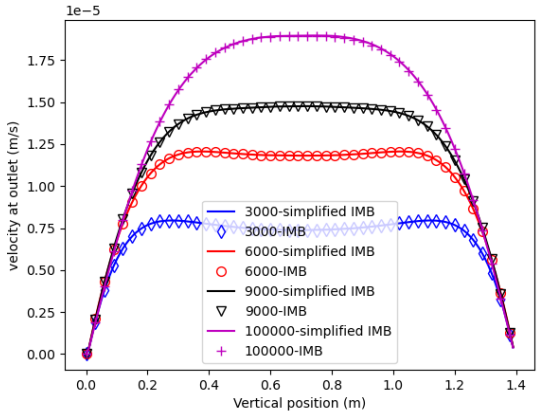

Fig. 14 Fluid velocity profiles at the outlet at different time steps

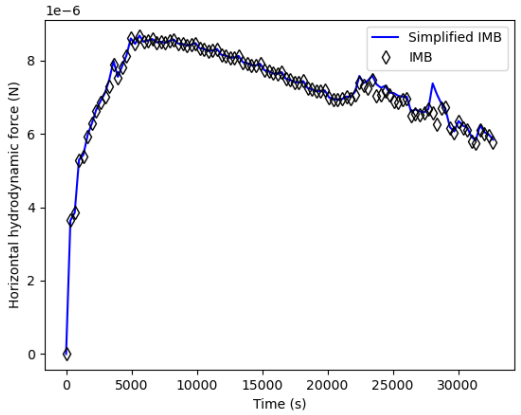

Fig. 15 Time histories of hydrodynamic force (particle 2)

400 Figure 14 quantitatively compares the velocity profiles at the outlet for four time instants by the enhanced and
401 simplified IMB schemes. It is found that the velocity profiles from the two schemes match very well. Next, the time
402 histories of the hydrodynamic force applied to particle 2 by both enhanced IMB and simplified IMB are examined
403 and showed in Figure 15. A generally very good agreement except for a few points between the enhanced IMB and

the simplified IMB can be seen. It should be highlighted that when two particles start overlapping with each other, it will result in the total area of solid particles at some nodes exceeding the nodal area, which could cause the stability issue if Equation (21) is not adopted in the original IMB. However, the simplified IMB is free of this issue. The mechanism of instability of the original IMB will be explained and discussed in detail in the next section. The robustness of both enhanced and simplified IMB schemes has been demonstrated by this special test case.

4 Discussions

In most existing IMB references, the treatment of multiple-covered nodes is seldom reported. Normally, two or more particles can intersect with one node, but overlap between particles should not happen at a node in reality. However, in DEM simulations, particles may be in overlap even if the lubrication is accounted for in a fluid-particle system due to the penalty-based contact treatment nature of DEM and its coupling with the fluid solver. In DEM, a small overlap is allowed and used to calculate contact forces between particles in contact. Besides, in a fluid-particle system involving strong coupling, due to the explicit time integration used in DEM, a relatively large overlap could occur when hydrodynamic forces are much higher than contact forces. This may result in the total area of solid particles at some nodes exceeding the nodal cell area. Consequently, the denominator in Equation (19) may become an extremely small value, leading to a negative or extremely large weighting function and subsequently causing instability in LBM.

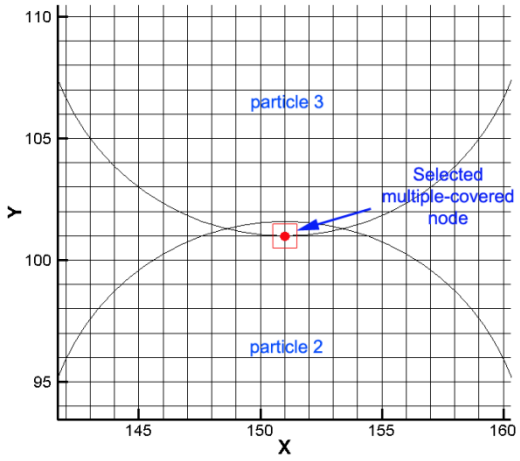

Fig. 16 Snapshot of an instable case with LBM mesh

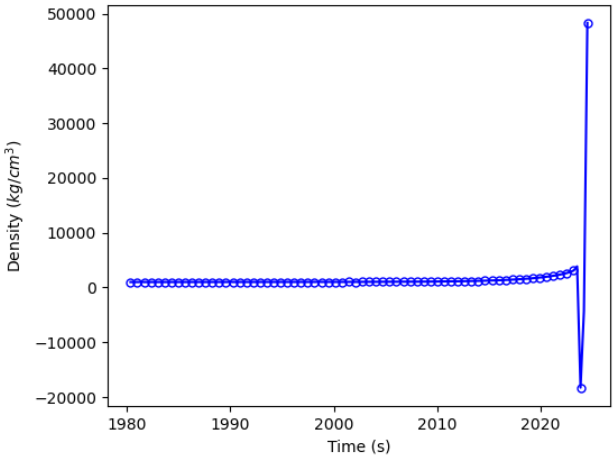

Fig. 17 Abnormal variation of density at the selected multiple-covered node

Take the special flow past cylinders in Section 3.4 for example, Figure 16 shows the snapshots of a case where an instable simulation using Equation (19) is encountered when the ratio of the total area of solid particles to the nodal area exceeds 1.0 in some nodes. The abnormal variation of the density at the selected node marked in red is given in Figure 17. Theoretically, the density should be around 1000 kg/cm^3, but a negative and extremely large value (over

40000) can be observed in the simulation due to the multiple-covered node in the original IMB. This issue can be overcome by the treatment of the weighting function in Equation (19) for the multiple-covered situations, and the proposed form in Equation (21) is a feasible solution. Furthermore, to make the velocity field of the fluid smooth, the fluid velocity of a multiple-covered node is the solid ratio weighted average from all the related solid particles (See equation (23)). It should be noticed that the linear form of the weighting function is free of such a stability problem.

Although the DEM-LBM-IMB technique has been extensively investigated in the past 20 years, the validation of accuracy is mainly performed based on fluid-stationary particle cases or single particle sedimentation. In this work, it is found that these simple cases are insufficient to validate the accuracy of DEM-LBM-IMB. At least, the DKT case or other complex simulations should be established as additional benchmarks. In addition, in most of DEM-LBM work only velocities and positions of solid particles are compared. This is found insufficient to examine the accuracy and stability of an IMB scheme, and the hydrodynamic force is shown to be a better quantity for validation in this work.

Finally, the computational efficiency of the enhanced IMB and the simplified IMB are compared. Table 2 presents the computational costs for the 3 test cases. For the DKT and the special flow past cylinders example where only a few movable particles are involved, the simplified IMB can only save very limited computing time. With the increase of particles number as in the multiple-particle sedimentation, the percentage of the saved time increases.

Although the computational efficiency is not significantly improved, the simplified IMB is much easier to be implemented than the enhanced IMB in the framework of DEM-LBM. It avoids the complicated treatment of the weighting function and additional loops over all particles, and there is no need to identify and counter multiple-covered nodes.

Table 2 Computational cost of simulations using IMB and simplified IMB

	DKT	Flow past cylinder	Multiple-particle sedimentation
Enhanced IMB	188 s	254 s	8617 s
Simplified IMB	186 s	249 s	8183 s
Saved time	1.1%	2.0%	5.0%

5 Conclusions

This work has presented and analyzed an instability issue of DEM-LBM-IMB for multiple-covered nodes, where several particles may intersect with one lattice nodal cell. An enhanced IMB formulation has been proposed to resolve the issue. Another contribution of this work is the development of a simplified but general IMB scheme to overcome issues encountered in the original IMB, and to avoid the complicated treatment of the weighting function and related additional loops over particles. Validations of the enhanced and simplified IMB methods have been carried out using a series of numerical tests with increasing complexity. The following conclusions can be drawn.

1) The instability of the original IMB stems from a possible very small denominator in the nonlinear form of the weighting function in IMB for a moving multiple-covered particle. This may happen when the total area of solid particles at a multiple-covered node exceeds the nodal cell area, leading to an extremely large weighting function and subsequently causing large/negative fluid density distribution functions.

2) An enhanced IMB with a special treatment of the weighting function and using the averaged velocity for a multiple-covered particle is proposed. Its accuracy and stability are demonstrated by the tests.

3) To simplify the code implementation, a simplified IMB scheme is further proposed. It is proved to be, to a certain degree, more efficient with a reasonable accuracy than the enhanced IMB.

4) For the validation of stability of the DEM-LBM method with various coupling schemes, the hydrodynamic force of a particle, which is a high-order quantity compared to particle position and velocity, is more important and should be examined.

References

[1] Clausen, J.R., Reasor Jr, D.A. and Aidun, C.K., 2010. Parallel performance of a lattice-Boltzmann/finite element cellular blood flow solver on the IBM Blue Gene/P architecture. Computer Physics Communications, 181(6), pp.1013-1020.

[2] Lominé, F., Scholtes, L., Sibille, L. and Poullain, P., 2013. Modeling of fluid–solid interaction in granular media with coupled lattice Boltzmann/discrete element methods: application to piping erosion. International Journal for Numerical and Analytical Methods in Geomechanics, 37(6), pp.577-596.

[3] Tsuji, Y., Tanaka, T. & Ishida, T. 1992. Lagrangian numerical simulation of plug flow of cohesionless particles in a horizontal pipe. Powder Technology, 71, 239-250.

[4] O'Connor, R.I.M., Torczynski, J.R., Preece, D.S., Klosek, J.T. and Williams, J.R., 1997. Discrete element modeling of sand production. International Journal of Rock Mechanics and Mining Sciences, 34(3), pp.373-373.

[5] Wang, M., Feng, Y.T., Pande, G.N., Chan, A.H.C. and Zuo, W.X., 2017. Numerical modelling of fluid-induced soil erosion in granular filters using a coupled bonded particle lattice Boltzmann method. Computers and Geotechnics, 82, pp.134-143.

[6] Cheng, H., Luding, S., Rivas, N., Harting, J. and Magnanimo, V., 2019. Hydro-micromechanical modeling of wave propagation in saturated granular crystals. International journal for numerical and analytical methods in geomechanics, 43(5), pp.1115-1139.

[7] Goodarzi, M., Kwok, C. Y. & Tham, L. G. 2015. A continuum-discrete model using Darcy's law: formulation and verification. International Journal for Numerical and Analytical Methods in Geomechanics, 39, 327-342

[8] Zeghal, M. and El Shamy, U., 2004. A continuum-discrete hydromechanical analysis of granular deposit liquefaction. International Journal for Numerical and Analytical Methods in Geomechanics, 28(14), pp.1361-1383.

[9] Hu, H.H., 1996. Direct simulation of flows of solid-liquid mixtures. International Journal of Multiphase Flow, 22(2), pp.335-352.

[10] Zwick, D. and Balachandar, S., 2019. A scalable Euler–Lagrange approach for multiphase flow simulation on spectral elements. The International Journal of High Performance Computing Applications, p.1094342019867756.

[11] Qian, Y.H., d'Humières, D. and Lallemand, P., 1992. Lattice BGK models for Navier-Stokes equation. Europhysics Letters, 17(6), p.479.

[12] Cook, B.K., Noble, D.R. and Williams, J.R., 2004. A direct simulation method for particle-fluid systems. Engineering Computations, 21, pp.151-168.

[13] Boutt, D.F., Cook, B.K., McPherson, B.J. and Williams, J.R., 2007. Direct simulation of fluid-solid mechanics in porous media using the discrete element and lattice-Boltzmann methods. Journal of Geophysical Research: Solid Earth, 112(B10).

[14] Wang, M., Feng, Y.T. and Wang, C.Y., 2016. Coupled bonded particle and lattice Boltzmann method for modelling fluid–solid interaction. International Journal for Numerical and Analytical Methods in Geomechanics, 40(10), pp.1383-1401.

[15] Ladd, A.J., 1994. Numerical simulations of particulate suspensions via a discretized Boltzmann equation. Part 1. Theoretical foundation. Journal of fluid mechanics, 271, pp.285-309.

[16] Delenne, J.Y., Mansouri, M., Radjaï, F., El Youssoufi, M.S. and Seridi, A., 2011. Onset of immersed granular avalanches by DEM-LBM approach. In Advances in Bifurcation and Degradation in Geomaterials (pp. 109-115). Springer, Dordrecht.

[17] Mei, R., Luo, L.S. and Shyy, W., 1999. An accurate curved boundary treatment in the lattice Boltzmann method. Journal of computational physics, 155(2), pp.307-330.

[18] Tao, S., Hu, J. and Guo, Z., 2016. An investigation on momentum exchange methods and refilling algorithms for lattice Boltzmann simulation of particulate flows. Computers & Fluids, 133, pp.1-14.

[19] Peskin, C. S. 1977. Numerical analysis of blood flow in the heart. Journal of Computational Physics, 25, 220-252.

[20] Feng, Z. G. & Michaelides, E. E. 2004. The immersed boundary-lattice Boltzmann method for solving fluid-particles interaction problems. Journal of Computational Physics, 195, 602-28.

[21] Niu, X.D., Shu, C., Chew, Y.T. and Peng, Y., 2006. A momentum exchange-based immersed boundary-lattice Boltzmann method for simulating incompressible viscous flows. Physics Letters A, 354(3), pp.173-182.

[22] Uhlmann, M., 2005. An immersed boundary method with direct forcing for the simulation of particulate flows. Journal of Computational Physics, 209(2), pp.448-476.

[23] Wu, J. and Shu, C., 2009. Implicit velocity correction-based immersed boundary-lattice Boltzmann method and its applications. Journal of Computational Physics, 228(6), pp.1963-1979.

[24] Dash, S.M., Lee, T.S., Lim, T.T. and Huang, H., 2014. A flexible forcing three dimension IB–LBM scheme for flow past stationary and moving spheres. Computers & Fluids, 95, pp.159-170.

[25] Wang, Z., Fan, J. and Luo, K., 2008. Combined multi-direct forcing and immersed boundary method for simulating flows with moving particles. International Journal of Multiphase Flow, 34(3), pp.283-302.

[26] Wang, M., Feng, Y. and Qu, T., 2020. On the implicit immersed boundary method in coupled discrete element and lattice Boltzmann method. International Journal for Numerical and Analytical Methods in Geomechanics, 44(4), pp.516-532.

[27] Noble, D.R. and Torczynski, J.R., 1998. A lattice-Boltzmann method for partially saturated computational cells. International Journal of Modern Physics C, 9(08), pp.1189-1201.

[28] Cui, X., Li, J., Chan, A. and Chapman, D., 2012. A 2D DEM–LBM study on soil behaviour due to locally injected fluid. Particuology, 10(2), pp.242-252.

[29] Cook, B., Noble, D., Preece, D. and Williams, J., 2000. "Direct simulation of particle-laden fluids", in Girard, J., Liebman, M., Breeds, C. and Doe, T. (Eds), Pacific Rocks 2000, Balkema, Rotterdam, pp. 279-286.

[30] Feng, Y.T., Han, K. and Owen, D.R.J., 2007. Coupled lattice Boltzmann method and discrete element modelling of particle transport in turbulent fluid flows: Computational issues. International Journal for Numerical Methods in Engineering, 72(9), pp.1111-1134.

[31] Han, K., Feng, Y.T. and Owen, D.R.J., 2007. Numerical simulations of irregular particle transport in turbulent flows using coupled LBM-DEM. Computer Modeling in Engineering and Sciences, 18(2), p.87.

[32] Galindo-Torres, S.A., 2013. A coupled Discrete Element Lattice Boltzmann Method for the simulation of fluid–solid interaction with particles of general shapes. Computer Methods in Applied Mechanics and Engineering, 265, pp.107-119.

[33] Owen, D.R.J., Leonardi, C.R. and Feng, Y.T., 2011. An efficient framework for fluid–structure interaction using the lattice Boltzmann method and immersed moving boundaries. International Journal for Numerical Methods in Engineering, 87(1-5), pp.66-95.

[34] Leonardi, C.R., Owen, D.R.J. and Feng, Y.T., 2012. Simulation of fines migration using a non-Newtonian lattice Boltzmann-discrete element model: Part I: 2D implementation aspects. Engineering Computations, 29(4), pp.366-391.

[35] Wang, D., Leonardi, C.R. and Aminossadati, S.M., 2018. Improved coupling of time integration and hydrodynamic interaction in particle suspensions using the lattice Boltzmann and discrete element methods. Computers & Mathematics with Applications, 75(7), pp.2593-2606.

[36] Wang, M., Feng, Y.T., Wang, Y. and Zhao, T.T., 2017. Periodic boundary conditions of discrete element method-lattice Boltzmann method for fluid-particle coupling. Granular Matter, 19(3), p.43.

554 [37] Jones, B.D. and Williams, J.R., 2017. Fast computation of accurate sphere-cube intersection volume.
555 Engineering Computations, 34(4), pp.1204-1216.

556 [38] Wang, M., Feng, Y.T., Pande, G.N. and Zhao, T.T., 2018. A coupled 3-dimensional bonded discrete element
557 and lattice Boltzmann method for fluid-solid coupling in cohesive geomaterials. International Journal for Numerical
558 and Analytical Methods in Geomechanics, 42(12), pp.1405-1424.

559 [39] Wang, M., Feng, Y.T., Owen, D.R.J. and Qu, T.M., 2019. A novel algorithm of immersed moving boundary
560 scheme for fluid–particle interactions in DEM–LBM. Computer Methods in Applied Mechanics and Engineering,
561 346, pp.109-125.

562 [40] Wang, M., Feng, Y.T. and Wang, C.Y., 2017. Numerical investigation of initiation and propagation of
563 hydraulic fracture using the coupled Bonded Particle–Lattice Boltzmann Method. Computers & Structures, 181,
564 pp.32-40.

565 [41] Han, Y. and Cundall, P., 2017. Verification of two-dimensional LBM-DEM coupling approach and its
566 application in modeling episodic sand production in borehole. Petroleum, 3(2), pp.179-189.

567 [42] Wang, M., Feng, Y.T., Zhao, T.T. and Wang, Y., 2019. Modelling of sand production using a mesoscopic
568 bonded particle lattice Boltzmann method. Engineering Computations, 36(2), pp.691-706.

569 [43] El Shamy, U. and Abdelhamid, Y., 2014. Modeling granular soils liquefaction using coupled lattice Boltzmann
570 method and discrete element method. Soil Dynamics and Earthquake Engineering, 67, pp.119-132.

571 [44] Yang, G.C., Jing, L., Kwok, C.Y. and Sobral, Y.D., 2019. A comprehensive parametric study of LBM-DEM for
572 immersed granular flows. Computers and Geotechnics, 114, p.103100.

573 [45] Wan D, Turek S. 2006. Direct numerical simulation of particulate flow via multigrid FEM techniques and the
574 fictitious boundary method. Int J Numer Methods Fluids, 51(5):531-566.

575

576